AD-A091 991 <STEVENS INST OF TECH HOBOKEN NJ DEPT OF PHYSICS F/G 20/9
<STUDY OF THE ANATOMY OF THE X-RAY AND NEUTRON PRODUCTION SCALIN--ETC(U)
MAY 80 V NARDI, W PRIOR AFOSR-75-2754
UNCLASSIFIED <IT-P2002 AFOSR-TR-80-1140 NL

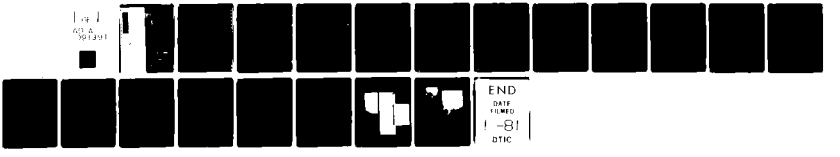

SIT-P2002-1980

LEVEL II

DTIC
ELECTE
S NOV 1 3 1980
D
C

DEPARTMENT OF PHYSICS

(14) SIT—P2002

(6) Study of the Anatomy of the X-Ray and Neutron Production Scaling Laws in the Plasma Focus.

(10) V. Nardi / W. Prior

(15) AFOSR-75-2754

(9) Final Report, AFOSR-Grant (75-2754)-80-0066
Period Oct 79 — Apr 80

(1) (30)

(11) 15 May 80

(12) 19

(16) 2301 (17) A7 (18) AFOSR

80 11 06 105

(19) TR-80-11

Approved for public release;
distribution unlimited.

AIR FORCE OFFICE OF SCIENTIFIC RESEARCH (AFSC)
NOTICE OF TRANSMITTAL TO DDC
This technical report has been reviewed and is approved for public release IAW AFR 190-12 (7b).
Distribution is unlimited.
A. D. BLOSE
Technical Information Officer

UNCLASSIFIED

SECURITY CLASSIFICATION OF THIS PAGE (When Data Entered)

REPORT DOCUMENTATION PAGE	READ INSTRUCTIONS BEFORE COMPLETING FORM
1. REPORT NUMBER: AFOSR-TR- 80 - 1140	2. GOVT ACCESSION NO.: AD-A091 994
3. RECIPIENT'S CATALOG NUMBER	
4. TITLE (and Subtitle): STUDY OF THE ANATOMY OF THE X-RAY AND NEUTRON PRODUCTION SCALING LAWS IN THE PLASMA FOCUS	5. TYPE OF REPORT & PERIOD COVERED: Final Oct. 1, 1979 - April 30,1980
	6. PERFORMING ORG. REPORT NUMBER: SIT-P 2002 -1980
7. AUTHOR(s): V. Nardi, W. Prior	8. CONTRACT OR GRANT NUMBER(s): AFOSR-75-2754
9. PERFORMING ORGANIZATION NAME AND ADDRESS: Stevens Institute of Technology, Physics/Engineering Physics Department, Castle Point Station, Hoboken, N. J. 07030	10. PROGRAM ELEMENT, PROJECT, TASK AREA & WORK UNIT NUMBERS: 61102F : 2301/A7
11. CONTROLLING OFFICE NAME AND ADDRESS: Department of the Air Force, Air Force Office of Scientific Res., Directorate of Physics, Bldg.410 Bolling Air Force Base, DC 20332	12. REPORT DATE: May 15, 1980
	13. NUMBER OF PAGES: 18
14. MONITORING AGENCY NAME & ADDRESS(if different from Controlling Office)	15. SECURITY CLASS. (of this report): Unclassified
	15a. DECLASSIFICATION/DOWNGRADING SCHEDULE

16. DISTRIBUTION STATEMENT (of this Report)

Approved for public release; distribution unlimited.

17. DISTRIBUTION STATEMENT (of the abstract entered in Block 20, if different from Report)

18. SUPPLEMENTARY NOTES

To be published with variation and with additional material on Physical Review, Issue A-5, Nov. 1980, by the American Institute of Physics, New York, N. Y.

19. KEY WORDS (Continue on reverse side if necessary and identify by block number)

Plasmoids, MeV-Deuterons, neutron yield, x-ray emission, electron beams, ion beams, energy spectrum, terawatt ions and electron beams, correlation coefficients, beam-induced damage, high-intensity ion and electron beams, dendrites, plasma focus, CR-39 plastic material, ion-track etching, ion imaging, Rogowski-coil measurements on electron beams.

20. ABSTRACT (Continue on reverse side if necessary and identify by block number)

Plasma-focus discharges at 20 kV (15 kJ) with a maximum yield of 10^9 neutron/shot in 6 torr deuterium, generate high-density plasmoids and collimated deuteron and electron beams. The maximum net current of the electron beam by Rogowski-coil signals (10 kA at 30 cm from the source) is instead observed at 3 torr. An image (contact print) of plasmoids which emit MeV deuterons is formed by the deuteron emission and it is revealed by etching deuteron tracks in a target of plastic material (CR-39). Ion-imaging with different energy filters discriminates

UNCLASSIFIED

20. Abstract continuation

between tracks of plasmoid ions and tracks of charged products of D-D fusion reactions. Ion-imaging can also discriminate plasmoid deuterons from MeV deuterons of a directed beam. The space-time structure of the D-D neutron source by collimated-neutron measurements is correlated with the structure of ion and of electron beams and with the structure of the plasmoids which are ejected along the electrode axis during the decay of the axial pinch. [1]

A detailed analysis has been completed on the internal structure of ions and electron beams which are ejected in opposite directions - 0^{o} and 180^{o}. Since the internal fine structure of ion and electron beams is similar at any distance $\gtrsim$ 6-50 cm from the source, a similar fine structure may exist in the beam source, as it is consistently indicated also by earlier observations on the fine structure of the pinch current sheath.

Final Scientific Report on AFOSR Grant (75-2754)-80-0066 for Period October 1, 1979 through April 30, 1980.

V. Nardi, W. Prior

This report investigates the correlation between the neutron (and x-ray) emission intensity and the intensity of the particle beams generated in a plasma focus discharge in deuterium as an extension of our previous work on scaling laws of x-ray and neutron production. The structure of dense plasmoids which emit MeV ions has been recorded by ion imaging with pinhole camera and contact print techniques. The plasmoids are generated in the same region in which particle beams, neutron and x-ray emission reach a maximum of intensity. Sharply defined boundaries of the ion-beam source and of plasmoids have been obtained by ion track etching on plastic material CR-39. A full length paper has been accepted for publication in the Physical Review, Issue A5, Nov. 1980. An invited paper "Generation of MA/cm^2 Electron and Ion Beams by Plasma Focus Discharges" was given by V. Nardi at the 1980 IEEE International Conference on Plasma Science, May 19-21, 1980 in Madison, Wisconsin (IEEE Conference Record, p. 73, University of Wisconsin).

P 1

Accession For	
NTIS GRA&I	☑
DTIC TAB	☐
Unannounced	☐
Justification	
By	
Distribution/	
Availability Codes	
Dist	Avail and/or Special
A	

1. Introduction

Plasma lumps (plasmoids) of linear dimensions $\ell \sim 1$ cm with an internal fine structure and a relatively-long life time τ are formed in a plasma focus discharge (15 kJ at 20 kV) and are ejected from the pinch region where ion and electron beams are generated. A plasmoid propagetes with a speed $v(\tau >> \ell/v)$ away from the hollow center electrode (anode) along the electrode axis in the same direction (0^0) of the ion beam[1]. The electron beam propagates in the opposite direction (180^0) through the hollow anode and in a drift tube which is filled with the same gas (D_2) and the same pressure p of the discharge chamber. Plasmoids in this experiments have sharply defined boundaries - with a drop in the particle density by one order of magnitude within a region $\Delta \lesssim 0.1$ mm - and an internal structure which are preserved during the plasmoid displacement from the source (pinch region) to the target. Plasmoid imaging - a contact print of the plasmoid on the target - is obtained by the MeV-ion emission from the plasmoid during the time of contact of the plasmoid with the target and by the related non-uniform density of ion tracks on the target.

Plasmoid with sharp boundaries and a long lifetime ($\tau \sim 0.1 - 1$ ns) have been observed in earlier experiments by image converter photographs (5 ns exposure by visible light) also at a late time of a plasma focus discharge , when the total current I on the electrodes had returned to the value $I \sim 0$ after the first current peak[2] ,at $t = T/2 \sim 4$ μs.

Ion-emission mode and life time of the observed plasmoids are consistent with the existence within the plasmoid of internal electric currents and of magnetic self-fields of high intensity (B) and with a fine structure on a space scale $\gtrsim \Delta$. Our observations suggest that a plasmoid can be identified with a current-sheath fragment which is ejected during the stage of decay of the axial pinch. If a fine structure exists in a plasmoid a similar structure can then be considered for the current sheath at different stages of the discharge. The ion beam which is ejected at 0^0 from the same axial region displays clearly a composite structure with ion clusters of linear dimensions $\sim 10 - 100$ μm.[1] Our observations on the fine structure of the electron beam are reported here and indicate that lumping in space and energy distribution, filamentation and filament clustering exist also in the electron beam. Similar structures are detected in the beam at any distance L_1 from the source ($L_1 \gtrsim 6$ cm). An implication is that the beam fine structure can be directly related with a similar fine structure of the current sheath. The bearing of a current sheath structure and strong self-fields - on the mechanisms which sustain the neutron emission can not be neglected and we consider it in the light of our fine-structure observations with a space resolution ~ 1 μm.

2. Experimental System and Methods.

The geometry of the system-plasma focus (PF) electrodes of diameters 10 cm (cathode) and 3.4 cm (anode), location of targets(for plasmoids, ion beam, electron beam)and electron-beam drift chamber-is reported in Fig. 1. The space distribution of the ion emission - ion beam, plasmoid contact print, D-D fusion protons - is obtained by NaOH etching of ion tracks in plastic targets (CR-39 plates, area 11 x 5 cm^2). CR-39 plates are covered with absorbing foils (mylar) of various thicknesses to screen out ions of energy lower than a chosen value and to discriminate tracks of fusion protons from MeV deuterons. Each CR-39 plate is exposed to a single discharge. Nuclear activation of BN, B(92% enriched B^{10}), C targets are also routinely used to assess typical energy distributions of the ion emission. The net electron beam current I_e is measured by two Rogowsky coils (RC) which encircle the drift chamber at two different locations. The net charge $Q_e = \int I_e dt$ is measured also by a Faraday cup method and is correlated with the neutron emission by each discharge. The filamentary structure of the electron beam is analyzed by beam-induced damage on plastic targets and on targets of special semiconductor material (Label/B) which are located inside the anode or in the drift chamber at any distance L_1 (6cm $\lesssim L_1 \leq$ 300 cm) from the anode front end. The electron-beam filaments carry along collectively-accelerated ions which are deposited on target. By using a thin plastic target (a single 125 μm thick polystyrene-PST-foil or a stack of 2-3 foils) the bulk of the electron beam with a dominant electron-energy value $E_e \sim$ 300 keV crosses the target. Collectively-accelerated ions and low energy ($\lesssim$ 50 keV) electrons are deposited and generate a non-uniform charge distribution on the target. The internal structure of an electron beam filament is revealed by local discharge processes (within the diameter $\hat{D}$ of the filament impact area - or filament marking - on the target) which are caused by this non-uniform distribution of charge. The different response of Label/B targets to beam deposition reveals details (others than filament internal-charge distribution) with a space resolution ($\sim$ 0.5 μm) better than by plastic targets.

3. Nuclear Tracks in Solids and Plasmoid Contact Print

The distribution of ion tracks is reported by photographs, FIG. 2. (a)-(e), of CR-39 plates etched with NaOH after exposure to a single discharge at 10 cm from the anode end (plate orthogonal to the electrode axis, 0^0, forward direction). (a) The two arks (ring structure) are formed by an ion track density corresponding to $\gtrsim 5 \times 10^6$ deuterons/cm^2 with energy of 2.4 Mev $\lesssim E \leq E_{max}$. E_{max} is determined by the sensitivity of the material and is not well known. Filter used was 50 μm of mylar (ρ = 1.38 g/cm^2). (b) Deuteron tracks (holes): Energy of the deuterons before passing through a 50 μm filter is $\gtrsim$ 2.4 Mev. This photograph corresponds to the relatively low surface track density region outside the sharp boundary of the two arcs in photograph (a). (c) Deuteron tracks (holes). This photograph corresponds to the high surface track density region of the two arcs in photograph (a). (d) Fusion proton tracks (holes). Mylar filter 125 μm thick. The average energy of the protons is about 3.0 Mev with the extra 0.5 Mev due to the average velocity of the center of mass of the reacting deuterons. The various hole diameters correspond to different proton velocities due to different center of mass velocities.

The track distribution in (a) may fit either an ion beam or a ring plasmoid; the distribution in (e) fits a plasmoid with a composite helix structure.

There are three reasons indicating that these tracks are due to fusion protons and not deuterons:

1. With a 100 μm mylar filter no tracks are observed. That is the deuterons that made the tracks with a 50 μm mylar filter have all been absorbed with the 100 μm mylar filter. The fusion protons have not been slowed down sufficiently by the 100μm mylar filter to produce etchable tracks. It is only by using a 125 μm mylar filter that the fusion protons are slowed down sufficiently to produce etchable tracks. Observation in other laboratories as well as our observations, on ion beams with independent methods (damage on metal plates and nuclear activation) consistently indicates that these beams are highly collimated (within a $\lesssim 6^0$ cone) in the 0^0 direction up to an energy $\cong$ 5 Mev. Consistently, the observed isotropy of these tracks (energy and typical track density) eliminate the possibility of a deuteron beam such that the energy distribution function of the deuterons after dropping to zero as the energy increases then suddenly makes a sharp increase in value for still higher values of the energy.

2. The surface track density is very uniform whereas with the previous deuteron tracks there is considerable structure.

3. Assuming (in agreement with the observation) an isotropic emission the surface track density agrees with the neutron production. No damage is observed on the mylar foil covering the CR-39 plate.

4. Current, Attenuation and Structure of the Electron Beam.

The structure of the ion beam within a $\lesssim 6^{\circ}$ cone on the electrode axis (in the forward direction, i.e. 0°) and the ion energy spectrum with a peak at~300 keV have been reported by previous work[5,7]. We are concerned here only with the electron beam ejected at 180° (from the same discharge region and at the same time of the ion beam emission)[8] and with the ions which are collectively accelerated by the electron beam in the same direction of the electron beam. The electron beam (and the ion beam at 0°) has a broad energy spectrum and carries $\gtrsim$ 10% of the capacitor bank energy by electrons with an energy from $\gtrsim$ 40 keV to several MeV. This spectrum has some variations from shot to shot as well as permanent features, specifically a peak at about 300-400 keV in all well-formed discharges[5] (i.e. a discharge - by using D_2 - with a neutron yield $n \gtrsim 0.5\ \bar{n}$, where $\bar{n}$ is the mean value of the neutron yield per discharge). For our system $\bar{n} \sim 2 \cdot 10^8$ neutron/shot (average over 10^2-10^3 shots in 6 Torr of D_2; for other gases a similar definition of well-formed discharge can be obtained in terms, e.g., of x-ray-energy-emission/shot). The electron beam propagates inside the hollow anode (length 15 cm) and then in the drift chamber (a pyrex pipe of 35 mm dia.) attached to the rear end of the anode (Fig. 1a). By beam-induced damage on targets inside the drift chamber we detect the filamentary structure of the electron beam, the internal structure of each filament (filament diameter $D \gtrsim$ 1-300 μm) and a nonfilamentary component of the same beam which is spatially uniform in a cylindrical region with cross-section diameter ~ 5 mm. Two anode configurations have been used: (i) fully open anode and (ii) partially closed anode with a circular aperture of 4 mm dia. at the center of the front end (a 3 mm thick plate) of the hollow anode (Fig. 1a).

By configuration (ii) a RC coil which is located downstream from the end of the focusing pipe P gives a typical value of the net e.b. current I_e which is much smaller (by a factor $\sim 10^{-1}$) than the typical value of the net current ($I_e \sim$ 1-10 kA) by configuration (i) or by configuration (ii) without focusing pipe P (the signal from a RC upstream from the end of the focusing pipe is always vanishingly small even when the target damage indicates a very intense beam). Target damage indicates that by (ii) with P the whole beam is formed by filaments. Tests with different values of the diameter of the anode aperture ϕ_2 indicate that the high energy component (> 300 keV) of the electron beam is generated near the electrode axis within a cylindrical region with diameter of ~ 3 mm,

length $\sim$ 1-2 cm, at the forward end of the anode. Each pulse of electron-beam net current I_e has rise time $\Delta t \gtrsim$ 1-10 ns to peak value $I_{eM} \sim$ 2-10 kA by Rogowsky-coil signals. By (i) $\nu/\gamma \gtrsim 0.6$ for one electron beam pulse, where ν is the number of beam electrons per classical electron radius e^2/mc^2 of beam length (the net value of ν/γ of a single filament in an electron beam pulse may have a quite different value; there are about 10^3 filaments in each electron beam). We have observed that the higher is the value of I_{eM}, the higher is the neutron yield n in a D_2 discharge (and the x-ray emission)[9]. This correlation between I_{eM} and n has been unambiguously established on 10^2-10^3 discharges. A similar, however more pronounced, correlation exists between beam charge $Q_p = \int_{2\Delta t} I_e \, dt$ and n.[9] First we have derived by a double time integration of RC signals the electron charge Q_p for each electron beam pulse. Then we have estimated the linear correlation coefficient $C(Q_p, n)$ between Q_p (e.g. for the first pulse) and the neutron yield in the same discharge in D_2. Our regressive analysis gives $C(Q_p,n) = 0.7$, with a probability $< 10^{-2}$ to obtain this value purely by chance (25 pulses have been examined at 6 Torr. RC_1 was at 26 cm from the anode front end). Max $Q_p = 10^{-3}$ Coulomb in a shot with $n = 2 \times \bar{n}$; mean value for first pulse $Q_{p_5} \gtrsim 4 \times 10^{-4}$C. Similar values for Q_p have been obtained by an independent method[5]. The total charge carried by the high-energy ($\gtrsim$ 300 keV) component of an electron-beam pulse was also measured after a PST (375 μm thick) with a Faraday-cup method with the same result (4×10^{-4} -10^{-3} Coulombs) as in Ref. 5. The velocity of propagation of the electron beam is $\gtrsim$ 76% of the speed of light c and it is obtained from the signals of two Rogowsky-coils RC_2, RC_3 (Fig. 1,a) surrounding the drift chamber with a distance between coils L = 150 or 300 cm. Our measurements of the attenuation α of the peak current by (i) of an electron beam pulse - $\alpha = [I_{eM}(RC_2) - I_{eM}(RC_3)]/I_{eM}(RC_2)$ where $I_{eM}(RC_2)$ is the current by RC_2 signal - give $\alpha \lesssim 0.25$ on 150 cm and $\alpha \gtrsim 0.5$ on 300 cm for a pulse of electrons with energy $\gtrsim$ 300-400 keV for 6 Torr of H_2 or D_2. This relatively-low decrease of net current of the beam is observed when the conducting ring G (at a distance 32 cm from the beam source is at floating potential (Fig. 1a). A higher attenuation (larger by about a factor 2; $\alpha \gtrsim 0.90$ over a distance of 300 cm) is instead observed if G is kept at ground potential. In this case the typical net current $I_{eM} \sim$ 1-10 kA of a pulse by RC_3 and RC_2 signals is however larger by a factor 5 than in the case of a

floating G. This higher value of I_{eM} and of α over a fixed traveling length L and the longer tail of each I_e pulse in the case of G grounded fit the idea that a floating G is charged by electron bombardment up to some negative voltage V_G. V_G then prevents beam electrons with a kinetic energy $< |eV_G|$ to propagate beyond G. Possible implications are (a) that these low-energy electrons contribute a substantial fraction of the beam net current and (b) that high-energy electrons (kin. en. $>> |eV_G|$) can propagate with small attenuation and with a substantial current neutralization.

It is compatible with (a) and (b) to consider that the nonfilamentary component of an electron beam can condense into filaments during the propagation of the beam in the drift chamber. By this process the high-current (nonfilamentary) component is depleted by increasing the current-neutralized (filamentary) component rather than by scattering in the background gas. All our data are consistent with the condensation picture. Targets of plastic materials (usually a polymethylmethacrilate - PMMA - 5 mm thick disc or a stack of one or more PST foils) have been used for different values of L_1 (6 cm $\leq L_1 \leq$ 300 cm). Label/B targets with value of the sublimation heat of $\sim$ 90 kcal/gatom are used to have a maximum of space resolution (better than 1 μm) of the internal structure of a filament. Target of plastic material are more suitable for detecting charge effects, voltage distribution and energy of collectively accelerated ions inside a filament. The filament-induced damage is detected in the form of rings, bubbles or holes on targets of plastic material (Fig. 3a). Craters and surface exfoliation of circular regions instead of bubbles is detected in Label/B (Fig. 3b).

The nonfilamentary component of the beam is detected by the formation of dendrites in a thick PMMA target which is ruptured through the irradiated volume (PMMA breakdown occurs from a planar region of accumulation of negative charge inside the target back to the bombarded external surface of the target. By observation of the dendrite-length distribution we have determined the dominant value of the electron energy - $\sim$ 300-400 keV - and the charge of the beam)[5]. This component of the beam is depleted and the dominant value of the electron energy in this component is somewhat lowered in the drift chamber for an increasing distance from the beam source. Dendrites formation is hardly observable for $L_1 \gtrsim$ 50 cm but shape and charge distribution of the nonfilamentary

component of the beam - which is the cause of dendrite formation - is still detectable for $L_1 \gtrsim 300$ cm by the isochromatic pattern (on a PST target foil) which is determined by the charge-induced stress in the foil[10]. We consider further only the filamentary component of the beam which tends to coalesce near the wall of the drift chamber (conf. (i) for $L_1 \sim 300$ cm. At this distance the beam has definitely changed its initial distribution which covers all the chamber cross-section to a new distribution by which the beam is concentrated on a ring 2-5 mm wide and with the same diameter of the chamber. This distribution is observed also by the x-ray image on conveniently-screened x-ray films which have been used as targets in some discharge. On a microscopic scale the filament-induced damage indicates that a filament can deposit an energy density $\gtrsim 200 J/cm^2$. The typical diameter δ of a filament by config. (i) is usually smaller by a factor $\gtrsim$ 2-3 than by using config. (ii) with a focussing pipe P. We further report only data from this latter arrangement (focuss. pipe dia. 7.8 mm) which give a more detailed picture of the internal structure of filaments (Fig. 3).

The circular cavity ($\sim$ 10-30 μm deep) at the border of a microscopic ring (Fig. 3a), its depth λ_o under the target surface, and the internal structure of each ring can be observed by light reflection through the transparent material of the target and by adjusting the microscope focal length on the chosen layer under the target surface. By a systematic inspection of more than 100 targets we conclude that each of these circular marks is caused by the ion deposition in the plastic when a beam filament reaches and crosses the target. The depth $\lambda_o \sim$ 10-30 μm of the groove indicates that ions with higher energy (1-2 MeV) are concentrated at the outer border of a microscopic ring and less energetic ions ($\lambda_o \sim$ 5 μm) are inside the ring. The filament electrons continue to propagate by further pinching after the ion deposition is completed and by forming a channel with diameter < 1-5 μm which punches its way through the target. We can in fact follow with the microscope this filament pattern from the bombarded surface to the rear surface of the target for about 90% of all the circular markings that we have examined. The positive charge per unit area of target at a ring location reaches the peak value over the time interval $\Delta \sim \ell/0.8xc \cong 1$ ns by which a filament of length ℓ penetrates the target surface.

Breakdown can then occur between the region below the target surface where the ions are trapped and the plasma outside the surface.[11] Breakdown can occur also along the target surface; there a positive Lichtemberg discharge pattern is etched (Fig. 3a)[12]. We have controlled to some extent the charge neutralization process of an ion ring by changing the target thickness and/or by collecting the electron beam on a metal plate immediately behind the target. By this procedure charge neutralization is achieved by breakdown through the whole thickness of the target. In this case the breakdown pattern between the ion-deposition cavity and the back side of the target (facing the electron collector plate; Fig. 1a) has a wiggling configuration somewhat different from the straight propagation channel of a pinched electron filament and surface discharge patterns as in Fig. 3a are not formed. Localized-discharge processes under the surface of a PST target may follow the nonuniform deposition of ions and low-energy (< 100 keV) electrons within the circular region of impact of a filament. The ring radial striations in Fig. 3a form the discharge pattern $\sim$ 10 μm under the target surface between the central region of the ring (where a positive charge is usually localized $\simeq$ 5 μm under the target surface) and the ring outer border where ion and electron deposition produces a circular cavity at a greater depth ($\sim$ 30 μm) under the target surface and low-energy electrons may exceed high-energy ions. On a Label/B (Fig. 3b) the regions of impact of bunches of collectively accelerated ions are detected as craters and holes ($\sim$ 1-10 μm dia.) which cluster in a circular (ring) pattern. The depth ($\simeq$ 10 μm) as in the center of the ring in Fig. 3b corresponds to a power deposition level $\sim$ 1 Tw/cm^2.

A substantial amount of the neutralization current of a filament can be contributed by collectively accelerated ions within a filament (high energy ions at the outer edge of the filament; lower energy ions near the filament central region; sed Fig. 3a). This is confirmed by a test with two Rogowsky coils, one (RC 1, Fig. 1b) before a 125 μm thick target of plastic material, the other (RC 2) after the target. The current detected by RC-2 is higher by a factor 4 ± 1 than the current detected by RC-1 (the distance between RC-1 and RC-2 was about 3 cm; coil calibration and an exchange of the two coils by different shots have been performed). A substantial fraction of the return current can be carried also by background-gas electronswhich are counterstreaming near the

surface of each filament. In fact a cloud of relatively-low-energy electrons which surrounds a filament produces - by baking the target surface - a tenuous halo which encirlces the deep mark of a filament on a Label/B target. This indicates that ion acceleration in the same direction of the electron beam is most effective within a filament and can be enhanced by the filament-formation process. The concentration of positive ions in filaments is consistently indicated by observation of: (a) the discharge pattern which originates from the ring-shaped mark of a filament on the target surface, as in Fig. 3a, is typical of a positive Lichtemberg discharge; specifically the surface-discharge arms are longer and more detailed than by a relatively small and thick-limbed negative Lichtemberg discharge.[12] (b) The distribution of the dark contamination dust which leaves circular white patches where the ion positive charge is concentrated. (c) The larger value of the electron-beam net current I_e downstream of a $\gtrsim$ 50 μm-thick plastic target with an arrangement as in Fig. 1b.

5. Nuclear Activation

Targets for nuclear activation are used to detect the high energy ($\gtrsim$ 200 keV) component of the ion beam at 0^0 and the collectively-accelerated ions by the electron beam at 180^0. Foil targets (a polypropylene foil 13x8 cm^2, 25 μm thick performing as a thick target for deuterons with energy $\lesssim$ 1 MeV) and thick graphite and BN targets have been used at 0^0, 10 cm from the anode end. Thick C and B^{10} targets have been used at 180^0, 50 cm from the anode front end, by configuration (ii) with focusing pipe diameter 4 mm. The observed β^+ decay of N^{13} nuclei from C^{12}(d,n) N^{13} reactions on 0^0 targets is $\gtrsim$ 200 times higher than the detector background. The observed activation corresponds to 10^{11}-10^{12} 1 MeV deuterons. The induced activation at 180^0 ($\sim$ 4 times the background level in some shots, negligible in other shots) gives $< 10^{10}$ of collectively accelerated deuterons.[13] The β^+ decay of C^{11} nuclei from B^{10} (d,n) C^{11} at 180^0 gives $\lesssim 10^9$ 0.5 MeV deuterons.

6. Discussion

We consider as vanishingly small the possibility that a localized source - rather than an plasmoid - ejects an ion beam with a suitable angular spread to generate the helical structure reported in Fig. 2(e) or other similar structures. The well defined values of ℓ, Δ in the plasmoid image - by contact print - indicate that either the 2.4 MeV deuterons are confined by a self field B_1 of high intensity (case I), or that the deuterons are accelerated to an energy $E_D \gtrsim 2.4$ MeV by an inductive field E on some distance $\lambda \lesssim \Delta, \ell$ when the plasmoid internal field of relatively-low intensity B_2 decays on a subnanosecond time interval δt (case II) by contacting the target surface. By equating the deuteron Larmor radius r_D with ℓ (or with Δ) a confining self field $B_1 = 205\ E_D^{1/2}(eV)/r_D(cm) \sim 3 \times 10^5$ G (or 3×10^7 G) is estimated for case I. In case II, by taking $\lambda = \ell$ (or $\lambda = \Delta$) we estimate from Maxwell's equation, $|E/\lambda| \sim |B_2/c\delta t|$, ($E_D = eE\lambda$), a field $B_2 \sim E_D\ c\delta t/\lambda^2$ which is substantially smaller than B_1 only if $\delta t << 10^{-11}$ sec. This estimate indicates that there are no good reasons to prefer case II above case I.

The filamentation of the electron beam increases during the beam propagation in the drift chamber, but is consistently detected also very close to the beam source. The beam filamentary structure is well fitting a beam source such as a current sheath with a texture of filamentary current channels, each channel with a diameter of the same magnitude of the diameter (~ 0.5 μm) of the smallest observed component of an electron beam filament.

References

1. W. H. Bostick, et al.: J. Nuclear Fusion Mat. Vol. 63 p. 356 (1976) and Proc. I.A.E.A. Conf. Plasma Physics and Controlled Nuclear Fusion Res., Innsbruck, 1978, Vol. 2, p. 143.

2. W. H. Bostick, V. Nardi, L. Grunberger, W. Prior, Proc. 10-th Int. Conf. Phenomena in Ionized Gases, Oxford, Sept. 13-15, 1971, Parsons & Co. Publ. p. 237. Specifically see Fig. 3 of this reference.

3. K. Molvig, G. Benford, W. C. Condit: Phys. of Fluids, Vol. 20, 1125 (1977). E. S. Weibel: Phys. Rev. Lett., Vol. 2, 83 (1959).

4. R. Lee, M. Lampe: Physical Review Lett., Vol. 31, 1390 (Dec. 1973).

5. V. Nardi, W. H. Bostick, J. Feugeas, W. Prior, C. Cortese: Prof. IAEA Conf. Plasma Physics and Controlled Nuclear Fusion Research (Innsbruck, 1978), Vienna 1979, Vol. 2, p. 143.

6. W. H. Bostick, V. Nardi, W. Prior: J. Plasma Physics, Vol. 8, 7 (1972). Same authors, Prof. IAEA Conf. (Berchtesgaden, 1976, see Ref. 5) Vol. 3, p. 497.

7. W. H. Bostick, V. Nardi, W. Prior, J. Choi, P. Fillingham, C. Cortese: J. Nuclear Materials 63, 356 (1976).

8. This is confirmed by collimated measurements on neutron and x-ray emission in D_2 discharges (ion and electron beam sources are also high-intensity sources of neutron and x-rays); see Ref. 6, 7.

9. The linear correlation coefficient for x-ray emission and neutron yield was estimated by previous work (W. H. Bostick, V. Nardi, W. Prior, F. Rodriguez-Trelles, C. Cortese, W. Gekelman in "Energy Storage, Compression and Switching", Plenum, New York 1976, p. 261).

10. D. Post: "Photoelasticity," in Measurement of Mechanical Properites, Part 2 (Techniques of Metal Research, Vol. 5), Bunshah R. F. edit., Interscience Publishers, New York 1971, Ch. 14.

11. G. A. Vorobev, V. S. Korolev: Sov. Phys. Tech. Phys., Vol. 21, 1222 (1976). PST targets evince a convenient polarity dependence of the nanosecond breakdown voltage U_{br} in a nonuniform (point electrode or filament-induced) electric field. The beginning of the voltage decay across a PST sample has a delay of a few nanoseconds after the developed discharge has crossed the sample thickness for a negative pulse; no delay is observed for a positive pulse which has U_{br} smaller by a factor $\gtrsim 2$ than U_{br} for the negative pulse. Consistently, we can expect that breakdown damage in the field of the deposited charge (with a positive net value) is not preceded in the same location by the occurrence of breakdown damage from the initially-negative pulse of a filament which approaches the target.

12. F. H. Merrill, A. von Hippel: J. Applied Phys., Vol. 10, 873 (1939).
G. C. Lichtenberg: Novi. Comment. Gott., Vol. 8, 163 (1777).

13. F. C. Young, M. Friedman: J. Appl. Physics, 46, 2001 (1975) and specifically Fig. 3 of this reference.
K. Wohlleben, E. Schuster: Radio Chimica Acta, 8, 78 (1967) and 12, 75 (1969) for C^{12}, $B^{10}(d,n)$ cross-section.

14. D. J. Johnson, J. R. Kerns: Applied Phys. Lett., Vol. 25, 191 (1974).

15. Vitkovitsky, I. M., Levine, L. S., Mosher, D., and Stephanakis, S. J., Appl. Phys. L. 23, 9 (1973).

Fig. 1

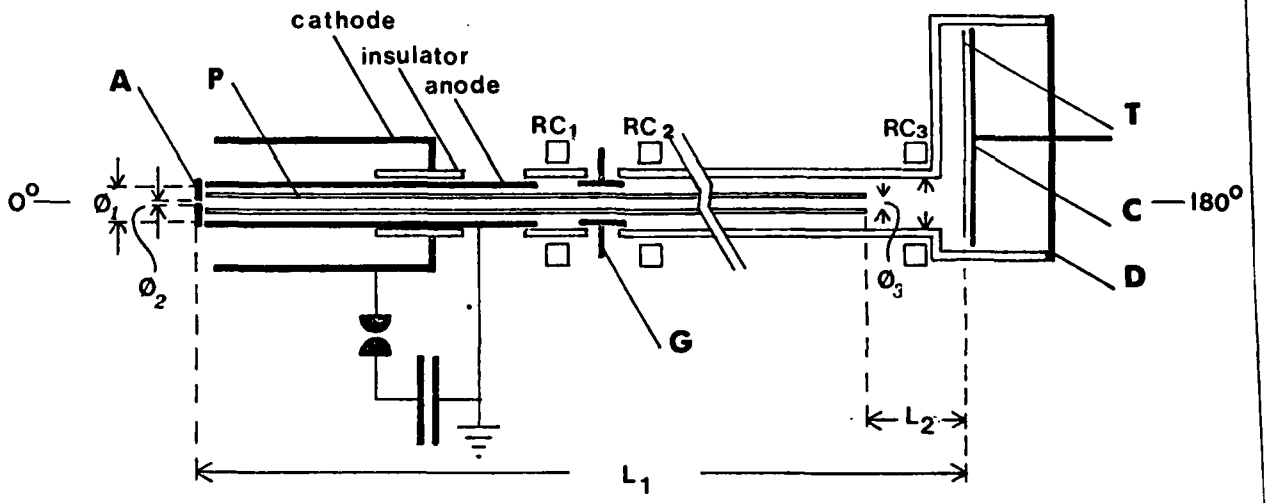

(a)

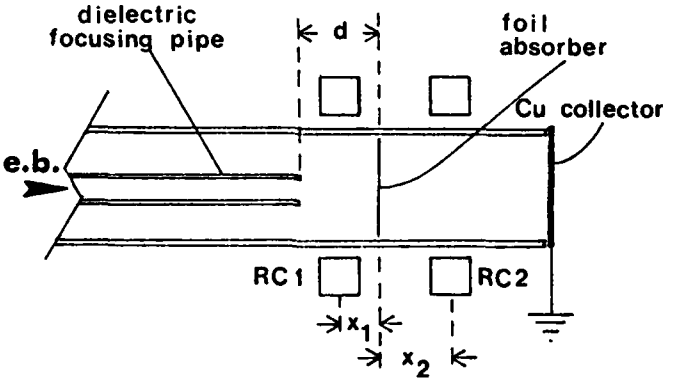

(b)

Fig. 1(a). Schematic view of inductive accelerator (plasma focus) and of the beam drift chamber (with the same filling gas and pressure, p=1-25 Torr, as in the discharge/beam-source chamber). A magnet (M_1) provides a 7 cm long B-field region. The net beam current I_e with a full-open anode (dia. ϕ_1 = 34 mm; configuration i) has a typical value 2-3 times larger than I_e by partially closing the anode with a disc (A, with an aperture of ϕ_2 = 4 mm dia. at the center; config. ii). By (ii) a pipe (P, dia. ϕ_3 = 7.8 mm or smaller) can be used to focus the beam; the distance between target and the end of P is L_2 = 1-8 mm when M_1 is not used. The support (C) of the target (T) is either a conducting plate or a floating grid. The beam charge is collected by C (or D) and is measured by discharging a connected capacitance in a convenient electric circuit. 1(b): Coils and target arrangement to measure variations of return current by ion absorption ($0 \leq d \leq 22$ mm; $9 \text{ mm} \leq x_1 \leq 25$ mm; $10 \text{ mm} \leq x_2 \leq 35$ mm).

Fig. 2

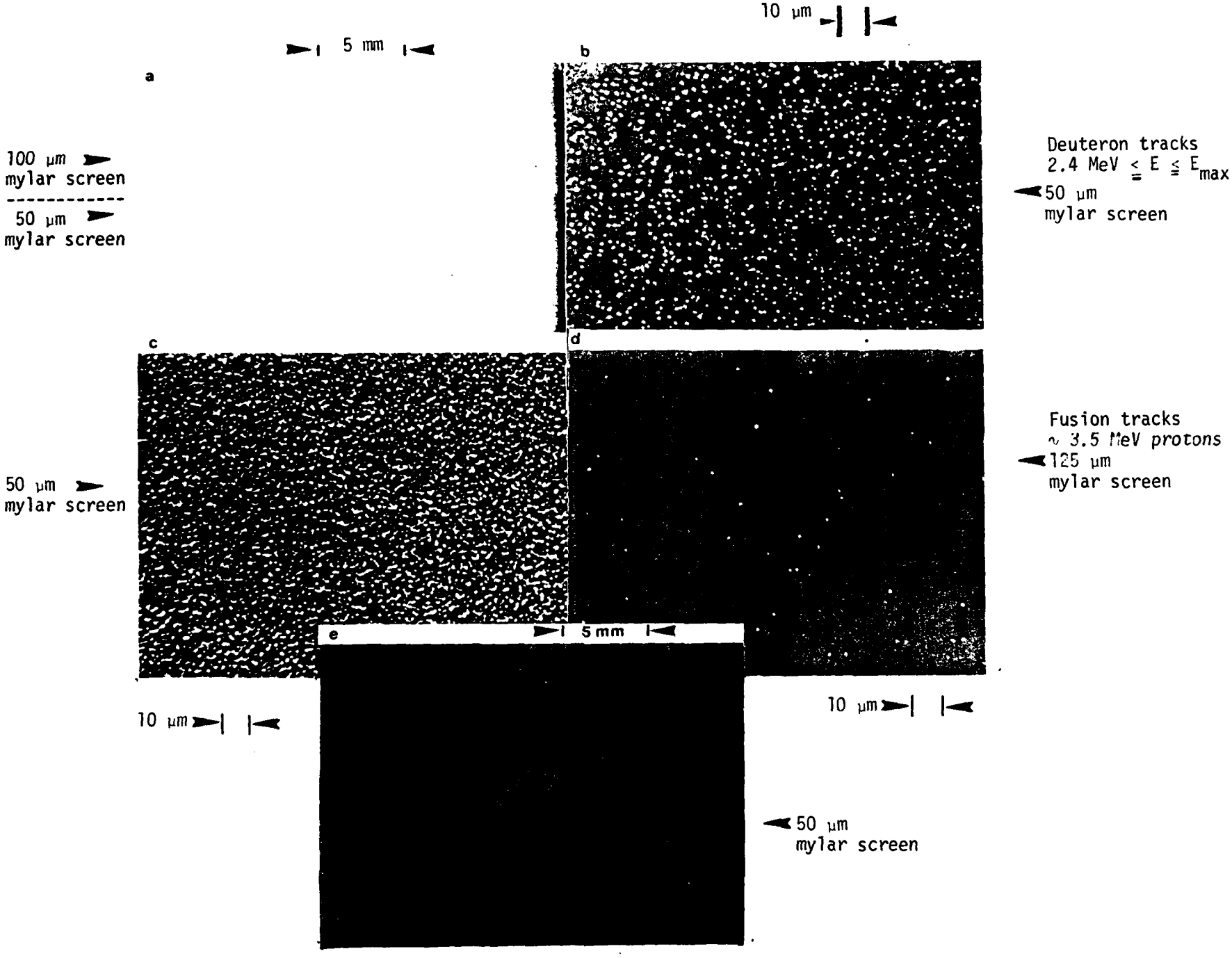
10 μm
5 mm
a
b
100 μm
mylar screen
50 μm
mylar screen
Deuteron tracks
2.4 MeV ≤ E ≤ E max
50 μm
mylar screen
c
d
50 μm
mylar screen
Fusion tracks
~ 3.5 MeV protons
125 μm
mylar screen
e
5 mm
10 μm
10 μm
50 μm
mylar screen

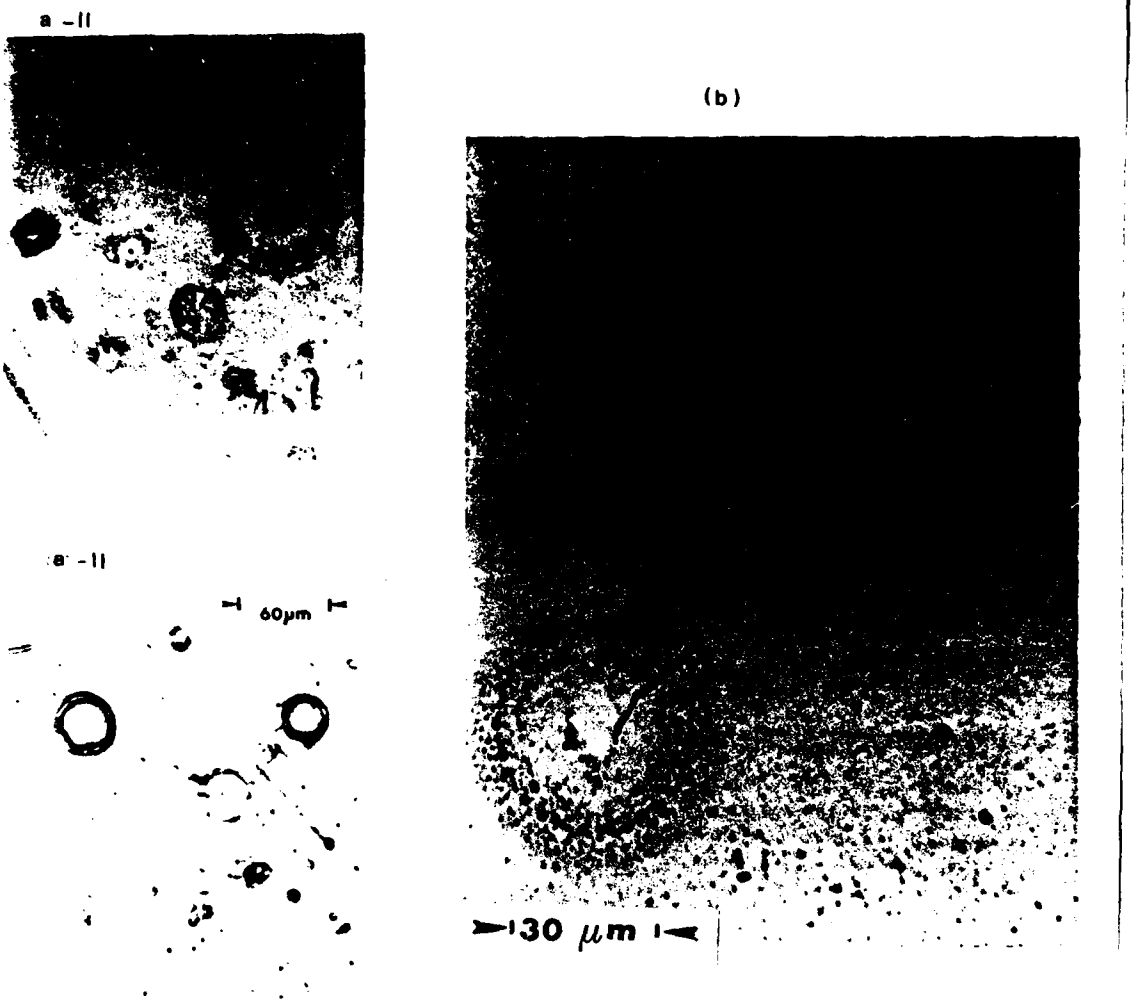

Fig. 3(a). Optical microscope photographs of beam-filament damage on PST targets (config. (ii), L_1 = 50 cm, L_2 = 3 mm). A grid was used as a target support. Exposure to a single discharge. (a)-I: Large (D∿4D̂) ring is formed by a discharge pattern 10 μm under the target surface: the exit hole of pinched electrons is visible at the center.
(a)-II: surface discharge-pattern connecting rings. The outer circle, in both left and right rings, is a cylindrical cavity ∿ 30 μm below the target surface.

(b): Optical-microscope photograph of electron-beam-induced damage on a target of semiconductor material (Lamel/B) at 180°, 50 cm from the plasma-focus beam source. The electron beam usually splits in a large number of filaments and of filament clusters ($\gtrsim 10^2$ filament clusters in a single discharge). The shallow damage (∿ 10 μm deep) in this photograph is produced by two clusters of filaments and reveals the internal fine structure of the electron beam.